Inorg. Chem. **2004**, *43*, 5103–5111

Emitting-State Displacements in Ligand-Centered Vibrational Modes in the *trans*-$[OsO_2(NCS)_4]^{2-}$ Complex Determined from Near-Infrared Luminescence Spectroscopy

John K. Grey,[†,‡] Ian S. Butler,[†] and Christian Reber*[,‡]

Department of Chemistry, McGill University, Montreal, QC H3A 2K6, Canada, and Département de Chimie, Université de Montréal, Montréal, QC H3C 3J7, Canada

Received February 8, 2004

Low-temperature luminescence spectra from three salts of the *trans*-$[OsO_2(NCS)_4]^{2-}$ complex exhibit highly resolved vibronic structure in both metal–ligand high-frequency O═Os═O (885 cm^{-1}) and lower-frequency Os–N(CS) (255 cm^{-1}) symmetric stretching modes as well as in a ligand-centered CS stretching mode (858 cm^{-1}). Band maxima range from 10000 to 12000 cm^{-1}, and spectra contain irregular frequency intervals that correspond to transitions from more than one origin and phonon sidebands. Experimental band shapes are distinctly different for all three compounds and are calculated assuming harmonic potential energy surfaces for both the ground and emitting states. Normal-coordinate offsets along all displaced vibrational modes are determined and compared for the three compounds. The analyses reveal emitting-state displacement of high-frequency ligand-centered (CS) and metal–ligand (O═Os═O) symmetric stretching modes, leading to observed high-frequency intervals (855–880 cm^{-1}) that do not match any frequencies determined from ground-state Raman spectra. The values for the high-frequency normal-coordinate offsets, $\Delta Q_{O=Os=O}$ and ΔQ_{CS}, were found to be on the order of 0.06 Å. Offsets along the 255 cm^{-1} Os–N mode varied noticeably between the three compounds and were largest for the compound with the largest value of ΔQ_{CS}.

Introduction

The lowest-energy absorption and luminescence transitions in many transition metal complexes occur between states that are localized on the metal center. These ligand-field (d−d) transitions are often interconfigurational and result in long vibronic progressions in metal−ligand vibrational modes corresponding to large emitting-state displacements along the metal−ligand normal coordinates. [1] We study the luminescence spectra of a series of *trans*-dioxo complexes of osmium(VI) with formal metal−oxo double bonds that show evidence for a displaced ligand-centered vibrational mode in the $^3E_g(d_{xz,yz}{}^1d_{xy}{}^1) \rightarrow {}^1A_{1g}(d_{xy}{}^2)$ (D_{4h} point group, *z* axis parallel to the O═Os═O moiety)[2] luminescence transition. The quantitative analyses of the spectra show the contribution of this mode to the overall band shape. The appearance of a ligand-centered vibrational mode is highly unusual in the luminescence spectroscopy of *trans*-dioxo metal complexes, which traditionally show progressions in metal−ligand modes only for their lowest-energy electronic transitions.[3−5]

Low-temperature luminescence spectra of the *trans*-$[OsO_2(NCS)_4]^{2-}$ complex in three different crystalline environments presented here exhibit remarkable resolution of vibronic structure in both high- and low-frequency vibrational modes, allowing for a full analysis of the resolved spectroscopic features. The most surprising characteristic is that the high-frequency vibronic interval (855−880 cm^{-1}) resolved in the luminescence spectra does not exactly match the ground-state Raman frequency for the totally symmetric O═Os═O stretching mode of 885 cm^{-1}. We present detailed spectroscopic and qualitative theoretical evidence for a significant displacement in the ligand-centered a_{1g} CS stretching vibration with a frequency of 858 cm^{-1}, only ∼30 cm^{-1} lower

* To whom correspondence should be addressed. E-mail: reber@chimie.umontreal.ca.
† McGill University.
‡ Université de Montréal.

(1) Landry-Hum, J.; Tessier, V.; Ernzerhof, M.; Reber, C. *Coord. Chem. Rev.* **2002**, *233*−*234*, 63.
(2) Miskowski, V. M.; Gray, H. B.; Hopkins, M. D. In *Advances in Transition Metal Coordination Chemistry*; Che, C.-M., Yam, V. W.-W., Eds.; JAI Press: Greenwich, CT, 1996; Vol. 1, p 159.
(3) Winkler, J. R.; Gray, H. B. *J. Am. Chem. Soc.* **1983**, *105*, 1373.
(4) Winkler, J. R.; Gray, H. B. *Inorg. Chem.* **1985**, *24*, 346.
(5) Savoie, C.; Reber, C. *J. Am. Chem. Soc.* **2000**, *122*, 844.

10.1021/ic049840v CCC: $27.50
Published on Web 07/13/2004

than the metal−ligand O═Os═O symmetric stretching frequency. The emitting-state displacement of both the O═Os═O and CS high-frequency modes leads to the observed discrepancy in the high-frequency interval, which is a consequence of the "missing mode effect" or MIME.[6,7] All vibronic band shapes are quantitatively analyzed using the time-dependent theory of spectroscopy with two potential energy surfaces representing the lowest spin−orbit component of the ^3E_g state as the initial state and the $^1A_{1g}$ ground state as the final state of the transition. The detailed spectra and analysis allow us to extract the individual contributions of both the O═Os═O and the ligand-centered CS stretching modes to the high-frequency interval.

Experimental Section

Three salts of the *trans*-$[OsO_2(NCS)_4]^{2-}$ complex were prepared using modified literature methods,[8−10] and starting materials were obtained from Aldrich and used as received. The three compounds are herein described using the following notation: (1) *trans*-$[OsO_2(NCS)_4](n\text{-}Bu_4N)_2$, **TBA**; (2) *trans*-$[OsO_2(NCS)_4](PPh_4)_2$, **PPH**; and (3) *trans*-$[OsO_2(NCS)_4](Ph_3PNPPh_3)_2$, **PPN** (PPN = bis-triphenylphosphoranylidene ammonium).

TBA. $K_2OsO_4{\cdot}2H_2O$ (0.04 g, 0.1 mmol) was dissolved in methanol to which was added a methanolic solution of KSCN (0.1 g, 1 mmol) along with tetrabutylammonium chloride (0.25 g). The pH of the solution was lowered by the dropwise addition of dilute glacial acetic acid, resulting in a color change from blue to a light brownish-yellow tint. The solution was placed in an 2-propanol/dry ice mixture (approximately −30 °C) for 4 h, where the compound precipitated as small, light beige crystals. Following filtration, the crystals were dissolved in dichloromethane, washed three times with distilled water, and dried with calcium chloride. The dichloromethane was evaporated in vacuo, yielding a reddish-brown residue that was dissolved in acetone and layered with diethyl ether. After 24 h at 4 °C, small reddish-brown needlelike crystals formed. Anal. Calcd for $OsO_2N_6C_{36}S_4H_{72}$: C, 46.02; N, 8.95; S, 13.60; H, 7.72. Found: C, 46.31; N, 8.99; S, 12.75; H, 7.85.

PPH. This compound was prepared by dissolving $K_2OsO_4{\cdot}2H_2O$ (0.07 g, 0.2 mmol) and PPh_4Br (0.36 g) in 2 M HCl; upon addition, *trans*-$[OsO_2(Cl)_4](PPh_4)_2$ precipitated immediately as small beige colored crystals along with KBr. This compound was separated and dissolved in acetone to which was added a solution of KSCN (0.21 g:2 mmol) in a minimum amount of distilled water. The solution was allowed to evaporate in air, yielding large dark brown crystals, which were recrystallized with acetone at 4 °C. Anal. Calcd for $OsO_2N_4C_{52}S_4H_{40}$: C, 55.10; N, 4.96; S, 11.30; H, 3.56. Found: C, 54.63; N, 5.09; S, 11.08; H, 3.49.

PPN. This compound was prepared in the same manner as **TBA** except that bis-triphenylphosphoranylidene ammonium chloride (0.12 g) was substituted for tetrabutylammonium chloride.

Spectroscopic Methods

Luminescence spectra were measured using two different instruments. The first system was a single-channel, step-scan spectrometer, and the 458, 488, and 514.5 nm lines of an argon ion laser (Spectra-Physics Stabilite 2017) were used to excite crystalline samples inside a continuous-flow cryostat (Oxford CF1204). Luminescence was collected and dispersed by a 0.5-m monochromator (SPEX 500 M, 600 lines/mm) with a long-pass filter to remove the excitation (Schott RG 645). Emitted light was modulated with an optical chopper (400 Hz) and detected with a liquid-N_2-cooled Ge photodiode (ADC 403UL) or photomultiplier tube (Hamamatsu R406) connected to a lock-in amplifier (Stanford Instruments SR 510 or SR 830). An in-house program was used to reject spikes in the luminescence signals measured with the Ge photodiode by sampling a preset number of data points and rejecting outlying values.[11] Because of the low signal-to-noise ratios of the photodiode detector for wavelengths shorter than 800 nm, a microscope-based system with a sensitive CCD camera was employed with argon ion (488 and 514.5 nm) and He−Ne (633 nm) laser excitation. Samples were placed under vacuum and cooled in a liquid helium microscope cryostat (Janis ST 500). Each compound has identical overall band shapes when excited with different wavelengths, and spectra recorded with both spectrometers can be superimposed to compare overlapping features. This is important because the two spectrometers have largely varying spectral sensitivities over the wavelength range studied. All spectra were corrected for instrument response with a tungsten lamp (Oriel 63350) using a literature procedure.[12]

Raman spectra of the *trans*-dioxo osmium(VI) complexes were obtained from the microscope spectrometer described above. Resonance Raman spectra of **PPH** at room temperature were measured on a double-monochromator (SPEX 14018, 0.75 m) system with single-photon-counting detection (SPEX DPC-2). The 458, 476, 488, and 514.5 nm lines of the argon ion laser were used as excitation sources, and the scattered light was collected at 90° and focused onto the slits of the monochromator. The excitation wavelengths are on or near resonance with the $^1A_{1g} \rightarrow {}^1E_g$ band, and excitation profiles were obtained for the O═Os═O and CS totally symmetric stretching vibrations from the integrated areas of the Raman bands, with the 995 cm^{-1} vibration of the PPh_4^+ counterion as an internal intensity standard. Infrared spectra of the title compounds were measured with an FT instrument (BioRad FTS 3000FX), and samples were dispersed in KBr and pressed into a pellet. UV−vis absorption spectra were obtained with a Varian Cary 5E spectrometer. Samples were cooled in the continuous-flow cryostat, and all spectra reported are unpolarized. Neutral-density filters were placed in the reference beam to keep the optical densities at a measurable level. Luminescence lifetime measurements were obtained using a Nd^{3+}:YAG pulsed laser (Continuum Minilite II, 5−10 ns pulse width) operating in either doubled (532 nm) or tripled (355 nm) output. The luminescence was collected and detected using the step-scan spectrometer described above. Decay traces were averaged and saved on a digital oscilloscope (Tektronix TDS 380) and least-squares routines were used to fit and assign decay.

Spectroscopic Results

Low-temperature single-crystal luminescence spectra of the *trans*-$[OsO_2(NCS)_4]^{2-}$ complex in three different crystalline environments are shown in Figure 1: **TBA**, top panel; **PPH**, middle panel; **PPN**, bottom panel. All spectra have weak intensities, even at low temperature, which indicates

(6) Tutt, L.; Tannor, D.; Heller, E. J.; Zink, J. I. *Inorg. Chem.* **1982**, *21*, 3858.
(7) Tutt, L.; Zink, J. I. *J. Am. Chem. Soc.* **1986**, *108*, 5830.
(8) Griffith, W. P.; Jolliffe, J. M. *J. Chem. Soc., Dalton Trans.* **1992**, 3483.
(9) Sartori, C.; Preetz, W. *Z. Anorg. Allg. Chem.* **1988**, *565*, 23.
(10) Stumme, M.; Preetz, W. *Z. Anorg. Allg. Chem.* **2000**, *626*, 1367.
(11) Oetliker, U.; Reber, C. *J. Near Infrared Spectrosc.* **1995**, *3*, 63.
(12) Davis, M. J.; Reber, C. *Inorg. Chem.* **1995**, *34*, 4585.

Table 1. Spectroscopic Quantities Determined from Luminescence Data Shown in Figures 1−4 and 6

parameter	TBA	PPH	PPN
lum maximum (cm^{-1})	11550	9900	11700
lum origin (cm^{-1})	12975	11650	13000
abs maximum (cm^{-1}) ($^1A_{1g} \rightarrow {}^3E_g$)	18500	17850	
Stokes shift (cm^{-1})	6950	7950	
lum lifetime (μs)	1.4 (9 K)	0.89 (10 K)	0.82 (85 K)
	1.3 (100 K)	0.79 (100 K)	0.65 (250 K)
	1.2 (200 K)	0.80 (200 K)	
vibronic intervals (cm^{-1})	870[a] (885 $\hbar\omega_{O=Os=O}$ and 858 $\hbar\omega_{CS}$)[b,c]	855[a] (885 $\hbar\omega_{O=Os=O}$ and 858 $\hbar\omega_{CS}$)[b,c]	880[a] (885 $\hbar\omega_{O=Os=O}$ and 858 $\hbar\omega_{CS}$)[b,c]
	255[a] (240, 251[c] $\hbar\omega_{Os-N}$)[b]	255[a] (258 $\hbar\omega_{Os-N}$)[b]	250[a] (251 $\hbar\omega_{Os-N}$)[c]

[a] Luminescence. [b] Ground-state Raman frequency (300 K). [c] Raman ref 10.

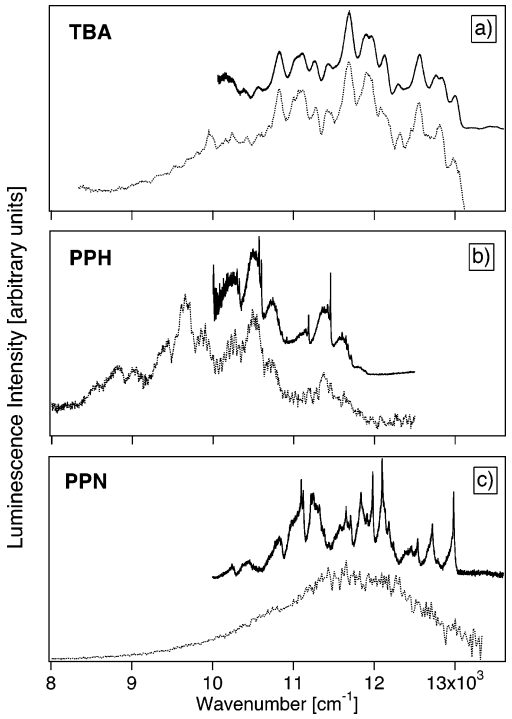

Figure 1. High-resolution 6 K luminescence spectra (top traces) and 5 K luminescence spectra showing the complete band (bottom traces) of (a) *trans*-$[OsO_2(NCS)_4](n\text{-}Bu_4N)_2$, **TBA**; (b) trans-$[OsO_2(NCS)_4](PPh_4)_2$, **PPH**; (c) *trans*-$[OsO_2(NCS)_4](Ph_3PNPPh_3)_2$, **PPN**.

efficient nonradiative deactivation of the emitting state, and show well-resolved vibronic progressions (up to four quanta) in a high-frequency interval (870 ± 5 cm^{-1} for **TBA**, 855 ± 8 cm^{-1} for **PPH**, 880 ± 5 cm^{-1} for **PPN**) and a low-frequency interval (ca. 255 cm^{-1}). The latter interval is in good agreement with the ground-state Raman band for the totally symmetric (a_{1g}) Os−N stretching vibration of 250−255 cm^{-1}, whereas the high-frequency interval does not exactly match any frequency in the Raman spectra of the three compounds. In the literature spectra of related compounds, the high-frequency progression interval corresponds to the O═M═O symmetric (a_{1g}) stretching frequency.[3−5] However, in the title compounds, two high-frequency vibrational modes are observed in the Raman spectra, the a_{1g} O═Os═O stretching mode at 885 cm^{-1} and the a_{1g} vibration of the ligand-centered CS stretching mode at 858 cm^{-1}, which are identical for all three compounds. Temperature-dependent luminescence lifetime measurements (λ_{exc} = 532 nm) for all three compounds reveal relatively short (~1 μs) single-exponential emitting-state decay, which is in qualitative agreement with previous observations in lower-energy emitting *trans*-dioxo complexes.[13]

Previous low-temperature (5−77 K) luminescence measurements reported for *trans*-dioxo osmium(VI) systems have often shown broad and unresolved bands or weakly resolved vibronic structure with intervals corresponding to the O═Os═O mode.[5,9,14] Each panel of Figure 1 shows the high-resolution spectrum as the top trace and the complete luminescence band as the bottom trace. The two spectra are recorded with different instruments or detectors, and intensities are not equivalent, whereas the luminescence band shapes are identical. All relevant spectroscopic parameters are listed in Table 1, and we discuss the spectra for each compound separately below.

Figure 1a shows the luminescence spectra recorded for the **TBA** compound at ca. 5 K with the band maximum energy at 11550 cm^{-1}. The high-resolution spectrum reveals a peculiar feature where the second peak of each cluster has a double maximum that gives rise to frequency intervals of 170 and 255 cm^{-1}. The latter value is in good agreement with both literature[9,10] and ground-state Raman values for the totally symmetric Os−N stretching mode. The 170 cm^{-1} interval is not repeated across the entire band and does not correspond to any frequency observed in the experimental Raman spectrum, although it is in good agreement with the frequency of an E_u vibration (171 cm^{-1}) reported in the literature IR spectrum of this compound.[9,10] Figure 2a displays the high-resolution luminescence spectrum with the single-crystal absorption spectrum at 5 K. The lowest-energy absorption band corresponds to the $^1A_{1g} \rightarrow {}^3E_g$ transition (18500 cm^{-1}), which is flanked by the more intense $^1A_{1g} \rightarrow {}^1E_g$ transition on the higher-energy side of the band. Details of the 5 K absorption spectrum of this compound are given in the Supporting Information. The effect of temperature on the **TBA** luminescence spectrum is shown in Figure 3a (λ_{exc} = 514.5 nm), and the spectra do not show an appreciable change in the overall luminescence band intensity with increasing temperature. However, there is a noticeable change in the intensity distribution in the second member in each cluster (i.e., double maximum), possibly due to a transition built on a vibronic origin, a second emitting state, or a different emitting species. As temperature increases, the double maximum coalesces into one peak and blue shifts by approximately 40 cm^{-1} between 6−100 K, consistent with

(13) Savoie, C.; Reber, C. *Coord. Chem. Rev.* **1998**, *171*, 387.
(14) Yam, V. W.-W.; Che, C.-M. *Coord. Chem. Rev.* **1990**, *97*, 93.

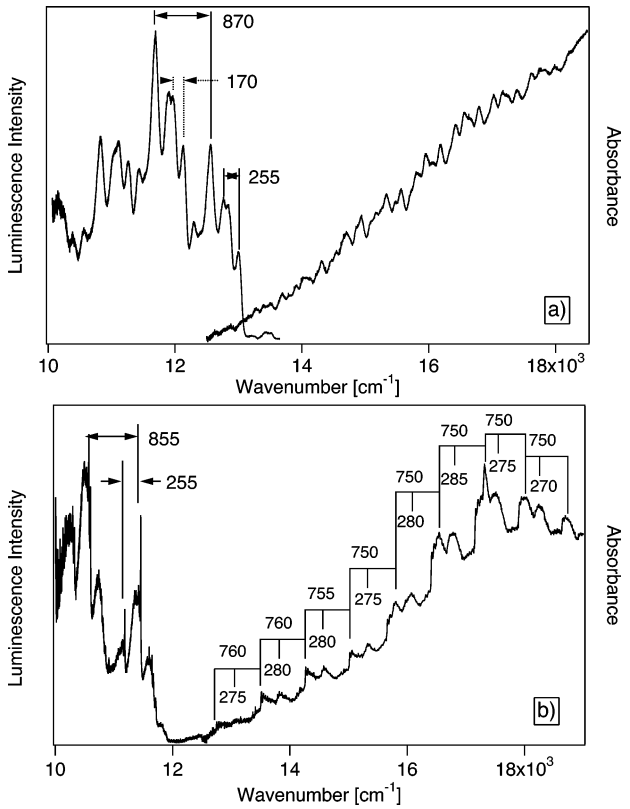

Figure 2. (a) High-resolution 6 K luminescence spectrum of **TBA** (λ_{exc} = 633 nm) with the resolved intervals indicated and 5 K single-crystal unpolarized absorption spectrum. (b) High-resolution 6 K luminescence spectrum of **PPH** (λ_{exc} = 633 nm) with the resolved intervals indicated and 5 K single-crystal unpolarized absorption spectrum showing the resolved frequency intervals of this state.

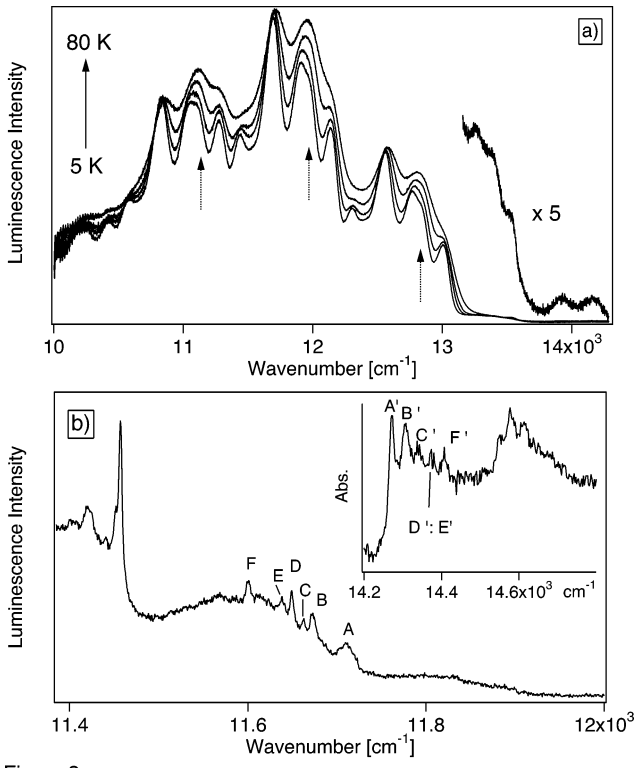

Figure 3. (a) Temperature-dependent luminescence spectra (λ_{exc} = 514.5 nm) of **TBA** at 6, 30, 50, and 80 K. Arrows show the increase of the intensity of the second peak with increasing temperature, and a high-resolution scan of the origin region is included (×5). (b) Origin region of the 6 K luminescence spectrum showing resolved phonon sidebands A−F and inset showing the corresponding region in the 5 K absorption spectrum with resolved phonon bands A′−F′.

progressions built on a vibronic origin. A high-resolution scan of the origin region of the luminescence is shown in Figure 3a (×5 bottom right) that reveals two very weak bands that might correspond to transitions allowed by a magnetic dipole mechanism. The appearance of a single quantum of the 170 cm^{-1} e_u mode leading to the double maximum on the second peak in each cluster strongly suggests a vibronic coupling mechanism whereby the formally spin- and parity-forbidden d−d luminescence borrows intensity from intense LMCT [E_u: $p_\pi(O)$] transitions observed between 300−400 nm.

Figure 1b shows the low-temperature luminescence spectra of the **PPH** compound. The low signal-to-noise ratio in the full spectrum (bottom trace) illustrates the very low quantum yields intrinsic to the *trans*-$[OsO_2(NCS)_4]^{2-}$ luminophore. Figure 2b shows the 6 K high-resolution luminescence spectrum and 5 K single-crystal unpolarized absorption spectrum of **PPH**. The absorption profile of this compound is similar to that of **TBA**, and these features are discussed in the Supporting Information. The average frequency interval of the dominant progression-forming mode in the 5 K luminescence spectra is 855 cm^{-1}, in excellent agreement with the ground-state Raman frequency of 858 cm^{-1} for the CS stretching mode. The overall spectral profile is also different from those of the **TBA** and **PPN** compounds, and the luminescence energy is lower by almost 1500 cm^{-1}. Figure 3b shows a high-resolution scan near the luminescence origin revealing low-frequency (40−100 cm^{-1}) phonon sidebands close to the beginning of each quantum of the lower-frequency progression, and the inset of Figure 3b shows a corresponding region in the 5 K absorption spectrum where a similar pattern is also observed. Similar features have also appeared in luminescence spectra of osmium(VI) nitrido complexes[15] and the isoelectronic *trans*-$[ReO_2(CN)_4]^{3-}$ complex,[4] revealing strong coupling between intramolecular and intermolecular motions. Excitation profiles for the O═Os═O and CS high-frequency modes generated from Raman measurements using variable-wavelength excitation show enhancements in both of these modes (Supporting Information). The mechanism of enhancement is probably due to both a preresonance effect with intense $p_\pi(O) \rightarrow d_{xz,yz}$ LMCT states and resonance with the $^1A_{1g} \rightarrow {}^1E_g$ transition of lower oscillator strength. From simple bonding considerations based on qualitative molecular orbitals, neither of these transitions is expected to lead to an enhancement of the CS mode, but spectroscopic results discussed in the following section clearly indicate the importance of this mode centered on the ancillary ligands.

Figure 1c shows both the high-resolution (top trace) and the complete luminescence (bottom trace) spectra at ca. 5 K. The high-resolution spectrum of this compound shows the best resolved vibronic structure. The dominant progres-

(15) Hopkins, M. D.; Miskowski, V. M.; Gray, H. B. *J. Am. Chem. Soc.* **1986**, *108*, 6908.

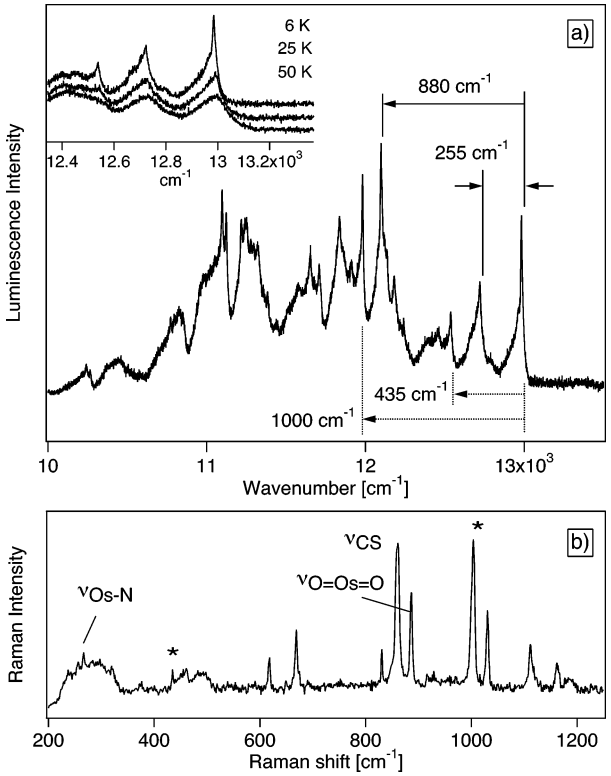

Figure 4. (a) High-resolution 6 K luminescence spectrum of **PPN** (λ_{exc} = 514.5 nm) with the resolved frequency intervals indicated with solid lines. Anomalous intervals appearing at 435 and 1000 cm^{-1} are indicated with dotted lines. The inset shows temperature-dependent luminescence spectra of this compound at 6, 25, and 50 K. (b) Room-temperature Raman spectrum (λ_{exc} = 633 nm) of **PPN** with the a_{1g} O═Os═O, CS, and Os−N bands labeled with asterisks indicating the 435 and 1000 cm^{-1} intervals.

sion interval is approximately 880 cm^{-1} with a lower-frequency progression of 255 cm^{-1}. The high-frequency progression interval is in good agreement with the ground-state Raman frequency of the O═Os═O stretching mode of 885 cm^{-1}. The high-resolution 6 K spectrum (Figure 1c) also shows evidence of phonon sideband structure; however, the spectrum is quite congested, making it difficult to definitively assign peaks to genuine progressions in low-frequency modes or transitions from multiple origins. Further comparison of the band envelope with those of the **TBA** and **PPH** complexes shows that, despite the similar energy range with **TBA**, the intensity distribution of the 255 cm^{-1} progression is noticeably different where the first maximum in each cluster is the most intense, indicating smaller emitting-state displacements along the Os−N normal coordinate.

Figure 4a shows the 6 K luminescence spectrum, with the 880 and 255 cm^{-1} intervals indicated. The first transition originates at 12975 cm^{-1}, and after the second quantum of the 255 cm^{-1} mode, an additional interval appears at 12540 cm^{-1} with progressions in the 880 and 255 cm^{-1} intervals built on this transition. The difference from the origin at 12975 cm^{-1} is 435 cm^{-1} (12540 cm^{-1}), and the Raman and IR spectra of this compound show weak bands corresponding to this frequency. Continuing across the band, there is another transition at 11980 cm^{-1} (∼1000 cm^{-1}), near the band maximum, with progressions in the 880 and 255 cm^{-1} modes built on this transition. Raman and IR spectra also reveal a peak corresponding to this frequency, and both the 435 and 1000 cm^{-1} frequencies are not repeated across the luminescence band. Furthermore, the progressions built on these origins have different temperature-dependent behavior. The 435 cm^{-1} mode is in reasonable agreement with an asymmetric (e_u) Os−NCS bending vibration of 470 cm^{-1} reported for the **TBA** compound,[10] and the 1000 cm^{-1} value closely matches a C═C vibration in the phenyl ring of the PPN^+ counterion. Temperature-dependent luminescence spectra show a rapid broadening of vibronic transitions leading to an overall decrease in resolution and intensity (shown in the inset of Figure 4a). There are also noticeable changes in the positions of resolved vibronic maxima; however, the signal-to-noise ratios also decrease rapidly with increasing temperature, making an analysis of these features very difficult. Figure 4b shows the ground-state Raman spectrum of this compound, where the a_{1g} O═Os═O, CS, and Os−N stretching vibration bands are indicated and asterisks highlight the 435 and 1000 cm^{-1} frequencies that correspond to the irregular intervals in the luminescence spectra described above. The appearance of a possible enabling mode in the Raman spectrum might be indicative of minor structural perturbations of the *trans*-$[OsO_2(NCS)_4]^{2-}$ luminophore in this compound.

Discussion

Vibronic Progressions in Metal−Ligand and Ligand-Centered Vibrational Modes. The low-temperature luminescence spectra in Figures 1−4 show remarkably well-resolved vibronic structure that enables a detailed analysis of the individual emitting-state distortions. The high-frequency intervals range between 855 and 880 cm^{-1}, which could arise from contributions from both the a_{1g} O═Os═O (885 cm^{-1}) and the CS (858 cm^{-1}) metal−ligand and ligand-centered modes, respectively. The displacement along the CS normal coordinate in the emitting state is clearly unexpected for a formal ligand-field transition that is largely localized on the osmium(VI) d orbitals, and to our knowledge, this case represents the first spectroscopic evidence for a Franck−Condon-active ligand-centered vibrational mode in the luminescence of *trans*-dioxo complexes.

We use DFT methods to calculate the molecular orbital surfaces for the HOMO and LUMO as well as vibrational frequencies to gain additional insight into the origin of this effect. These calculations are performed using the Gaussian 98 suite,[16] and the point group symmetry of the *trans*-$[OsO_2(NCS)_4]^{2-}$ complex is approximated as exactly D_{4h} but we do not impose symmetry constraints in the geometry optimization process. Figure 5 shows the results for the HOMO and LUMO surfaces generated in the DFT calculations with the coordinate systems indicated on both surfaces. These surfaces correspond well to the d_{xy} (b_{2g}: HOMO) and d_{xz}, d_{yz} (e_g: LUMO) orbitals. Judging from the large change in π^* electron density between the HOMO and LUMO levels, most notably on the *trans*-$[O═Os═O]^{2+}$ moiety, a large normal-coordinate displacement along the metal−oxo bonds is expected. Additionally, there are changes in π^*-electron density on the CS fragments of the NCS^- ligand.

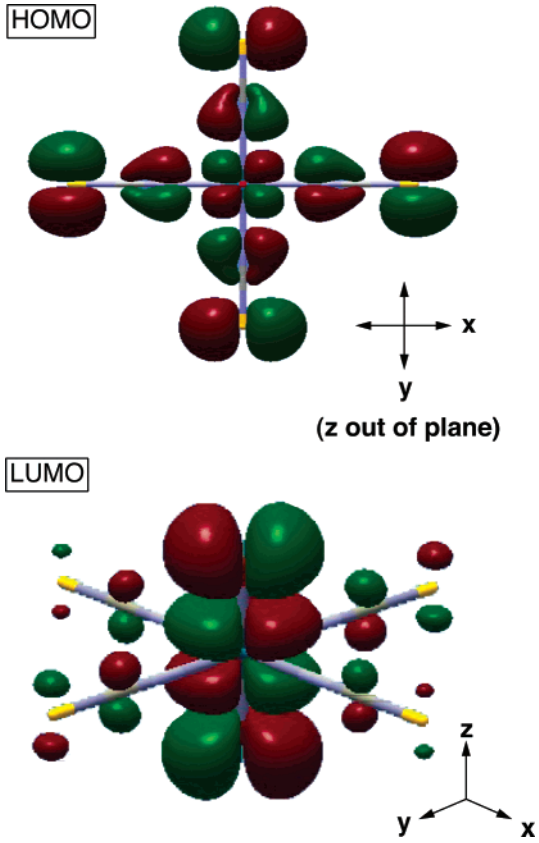

Figure 5. Molecular orbital surfaces generated from DFT calculations with Cartesian coordinate references given for each surface. The top picture is of the highest occupied molecular orbital (HOMO), and the bottom picture is the lowest unoccupied molecular orbital (LUMO).

In the HOMO surface shown in Figure 5, the π^* density on CS is in the *xy* (equatorial) plane of the molecule, whereas in the LUMO, the electron density has changed significantly (i.e., much lower in amplitude) and is perpendicular to this plane, qualitatively indicating possible changes in CS bond lengths in the emitting state. Calculations of vibrational frequencies are presented and compared with experimental results in the Supporting Information.

Calculation of the Vibronic Structure in the Luminescence Spectra. We use the time-dependent theory of luminescence spectroscopy[17−19] to calculate the experimental luminescence band shapes by fitting the intensity distributions within the overall band shape. The parameters used in the calculations are the normal-coordinate offsets, Δ_i (dimensionless units); the energy of electronic origin, E_{00} (cm^{-1}); the vibrational frequency for each displaced mode, $\hbar\omega_i$ (cm^{-1}); and the phenomenological damping factor, Γ (cm^{-1}), that defines the bandwidth of individual vibronic transitions. The values for Δ_i are adjusted to reproduce the individual intensity distributions for each displaced mode. We assume one emitting state and include three vibrational modes in these calculations, namely, the a_{1g} O═Os═O, CS, and Os−N stretching modes, and take their frequencies from both our own experimental and literature Raman spectra.[10] E_{00} is chosen as the energy of the first resolved peak in each progression, and in the **TBA** and **PPN** complexes, multiple origins are used to fit the experimental spectrum with progressions in the a_{1g} modes built on these origins. The initial and final states are represented as harmonic potential energy surfaces where it is assumed that (a) the vibrational frequencies, $\hbar\omega_i$, in the ground and excited states are identical; (b) there is no coupling between normal coordinates; and (c) the transition dipole moment is constant.

Initially, calculations were performed using only the O═Os═O and Os−N modes; however, agreement with experiment was poor because of the inability of the model to reproduce the high-frequency interval and intensity distributions of the low-frequency progressions in each compound. To account for the variations in the high-frequency interval between compounds, the ligand-centered a_{1g} CS stretching mode must be included. The relative contributions of the O═Os═O and CS modes can be estimated by calculating only the high-frequency interval using these two modes. Figure 6a shows an example for the **TBA** compound where the Δ values of both the a_{1g} O═Os═O (885 cm^{-1}) and CS (858 cm^{-1}) modes are varied to reproduce the observed high-frequency interval of 870 cm^{-1} in the 5 K spectrum. The appearance of a resolved frequency interval in luminescence spectra that does not have a matching value in the ground-state Raman spectrum has been termed the missing mode effect, or MIME.[6] The manifestation of the MIME in the title compounds is discussed in detail in the Supporting Information.

The appearance of the double maximum on the second member of each cluster in the **TBA** luminescence spectrum is unprecedented in the luminescence spectra of *trans*-dioxo complexes. Because there is no corresponding band in the ground-state Raman spectra, this feature is most likely a transition built on a different origin. Evidence for two different origins comes from the temperature-dependent luminescence spectra (Figure 3a), where the intensity and energy of the second member, i.e., the double maximum, changes as a function of temperature. We therefore interpret this interval as a vibronic origin built on the first peak of the double maximum starting at 12833 cm^{-1}. Figure 6a compares two spectra that are calculated using the three a_{1g} modes mentioned previously and the same values for Δ_i, $\hbar\omega_i$, and Γ (Table 2) with the high-resolution 6 K luminescence spectrum. The origin of the first calculated spectrum (dotted trace) is taken as the first peak in the main band

(16) (a) Frisch, M. J.; Trucks, G. W.; Schlegel, H. B.; Scuseria, G. E.; Robb, M. A.; Cheeseman, J. R.; Montgomery, J. A., Jr.; Stratmann, R. E.; Burant, J. C.; Dapprich, S.; Millam, J. M.; Daniels, A. D.; Kudin, K. N.; Strain, M. C.; Farkas, O.; Tomasi, J.; Barone, V.; Cossi, M.; Cammi, R.; Mennucci, B.; Pomelli, C.; Adamo, C.; Clifford, S.; Ochterski, J.; Petersson, G. A.; Ayala, P. Y.; Cui, Q.; Morokuma, K.; Malick, D. K.; Rabuck, A. D.; Raghavachari, K.; Foresman, J. B.; Cioslowski, J.; Ortiz, J. V.; Stefanov, B. B.; Liu, G.; Liashenko, A.; Piskorz, P.; Komaromi, I.; Gomperts, R.; Martin, R. L.; Fox, D. J.; Keith, T.; Al-laham, M. A.; Peng, C. Y.; Nanayakkara, A.; Gonzalez, C.; Challacombe, M.; Gill, P. M. W.; Johnson, B. G.; Chen, W.; Wong, M. W.; Andres, J. L.; Head-Gordon, M.; Replogle, E. S.; Pople, J. A. *Gaussian 98*, revision A.9; Gaussian Inc.: Pittsburgh, PA, 2001. (b) The LanL2DZ pseudopotential and basis set functionals and the RB3LYP method were used for the exchange-correlation energy term in the Kohn−Sham calculation.
(17) Zink, J. I.; Kim Shin, K.-S. In *Advances in Photochemistry*; Volman, D. H., Hammond, G. S., Neckers, D. C., Eds.; John Wiley: New York, 1991; Vol. 16, p 119.
(18) Heller, E. J. *J. Chem. Phys.* **1975**, *62*, 1544.
(19) Heller, E. J. *Acc. Chem. Res.* **1981**, *14*, 368.

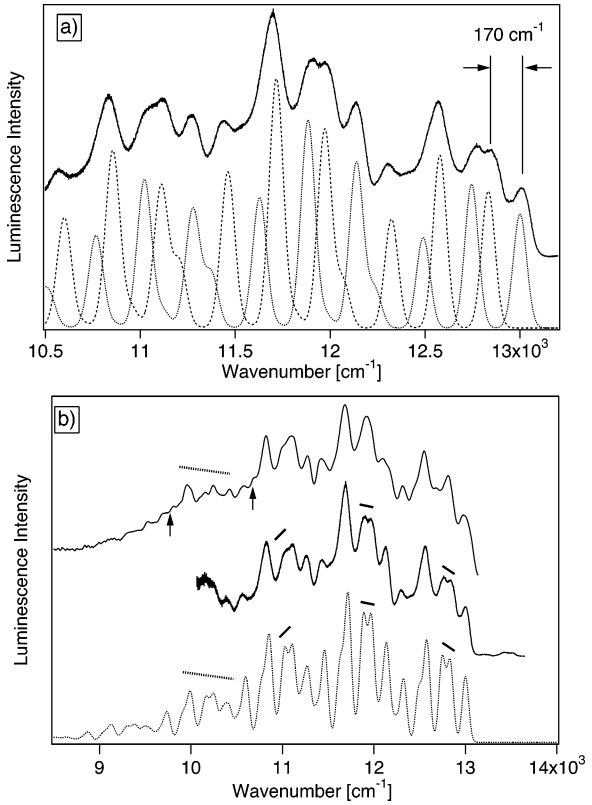

Figure 6. (a) Comparison of 6 K high-resolution luminescence spectrum of **TBA** (top trace) and three-mode (O═Os═O, CS, Os−N) calculated spectra. Two spectra are calculated based on different origins of 13000 cm^{-1} (···) and 12833 cm^{-1} (---) using identical offsets for the two spectra. (b) Comparison of 5 K luminescence spectrum (top trace), high-resolution 6 K luminescence spectrum (middle trace), and best-fit three-mode, two-origin calculated spectrum (bottom trace). Small solid sloping lines on the calculated spectrum and the high-resolution spectrum show the agreement between the experimental data and the calculated spectrum of the double maximum appearing on the second member of each cluster. Hatched sloping lines on the 5 K spectrum and the calculated spectrum show the effect of the varying intensity distribution of the 255 cm^{-1} Os−N progression. Arrows on the 5 K spectrum highlight shoulders that are reproduced in the best-fit calculated spectrum.

Table 2. Parameters Used for the Calculation of Luminescence Spectra

compound	**TBA**	**PPH**	**PPN**
E_{00} (cm^{-1})	I. 13000	11650	I. 12975
	II. 12830		II.[b] 12540
			III.[b] 11980
$\Delta_{O=Os=O}$, $\Delta Q_{O=Os=O}$	I.[b] 0.77, 0.038	1.22, 0.060	I. 1.30, 0.063
(dimensionless, Å)[a]	II. 0.77, 0.038		II.[c] 1.30, 0.063
($\hbar\omega_{O=Os=O}$ = 885 cm^{-1})			III.[c] 1.18, 0.058
Δ_{CS}, ΔQ_{CS}	I.[b] 1.76, 0.062	1.87, 0.065	I. 1.73, 0.061
(dimensionless, Å)[a]	II. 1.76, 0.062		II.[c] 1.73, 0.061
($\hbar\omega_{CS}$ = 858 cm^{-1})			III.[c] 1.34, 0.047
Δ_{Os-N}, ΔQ_{Os-N}	I.[b] 1.64, 0.078	1.87, 0.089	I. 1.22, 0.058
(dimensionless, Å)[a]	II. 1.64, 0.078		II.[c] 1.22, 0.058
($\hbar\omega_{Os-N}$ = 255 cm^{-1})			III.[c] 0.87, 0.030
Γ (cm^{-1})	25	70	10

[a] The formula for converting from dimensionless units is given by $\Delta Q_k = \sqrt{(N_A\hbar/4\pi^2 c\hbar\omega_k M)}10^8\Delta_k$, where N_A is Avogadro's number, $\hbar$ is Planck's constant in erg s, c is the speed of light in cm s^{-1}, $\hbar\omega_k$ is the frequency of the vibration in cm^{-1}, and M is the mass of the mode in g mol^{-1}. [b] The intensity of band I is scaled to 80% of its original value. [c] Intensities of bands II and III are scaled to 50% of their original vales to fit the experimental spectra.

(13000 cm^{-1}), and the first peak of the double maximum (12833 cm^{-1}) is the second origin (hatched trace). The first

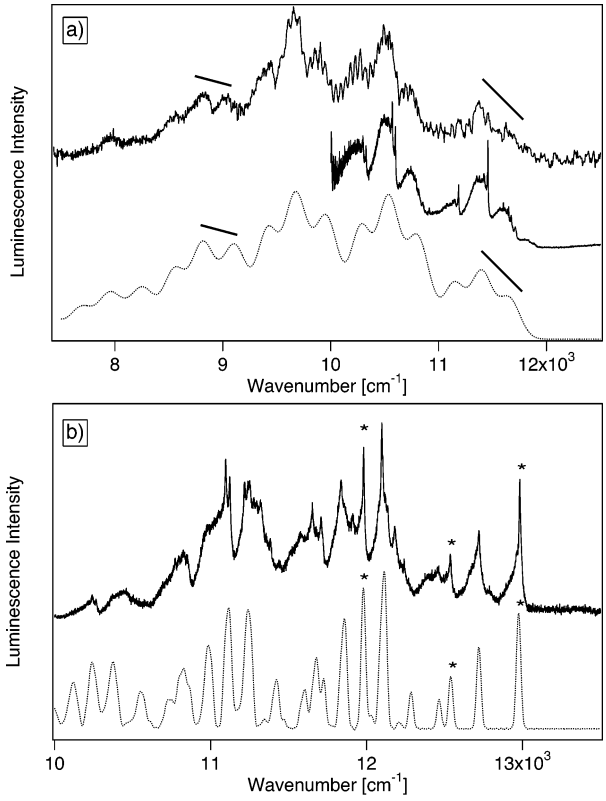

Figure 7. (a) Comparison of the 5 K luminescence spectrum (top trace) and the high-resolution spectrum (middle trace) of **PPH** with the best-fit calculated spectrum consisting of progressions in the a_{1g} O═Os═O, CS, and Os−N modes (bottom trace) with one origin at 11650 cm^{-1}. Sloping solid lines on the first and fourth clusters show the agreement between the calculated spectrum and experimental spectra. (b) Comparison of the 6 K high-resolution spectrum of **PPN** and the best-fit three-mode calculated spectrum. Three spectra are calculated with each origin indicated with an asterisk and are multiplied by an appropriate factor to obtain the proper intensity ratio within each spectrum.

spectrum (E_{00} = 13000 cm^{-1}) is multiplied by an appropriate factor to reproduce the overall intensity ratio of the first peak relative to that of the spectrum built on the second peak, which phenomenologically accounts for the total intensities of both electronic transitions, and the two spectra are added to obtain the total calculated spectrum. Figure 6b shows the best-fit total spectrum using the two-origin model (bottom trace) with the high-resolution 6 K spectrum (middle trace) and the 5 K overall spectrum (top trace). The best-fit spectrum shows excellent agreement with both experimental spectra, where the intensity distribution of the double maximum is replicated across the entire luminescence band (indicated by the small sloping solid lines) and the intensity distributions of each cluster are in very good agreement with the overall band envelope upon comparison with the 5 K total spectrum (illustrated with the hatched sloping lines for the third cluster). Upward pointing arrows on the 5 K spectrum point out small resolved shoulders on the lower-energy side of the third member of the 255 cm^{-1} progression that are also reproduced in the best-fit spectrum.

Figure 7a shows the 5 K luminescence spectrum (top trace) and calculated spectrum of **PPH** (bottom trace). The calculated spectrum was obtained using the totally symmetric O═Os═O, CS, and Os−N modes with one origin. We do

not attempt to reproduce the fine structure corresponding to phonon sidebands in the high-resolution spectrum and calculate only the overall band envelope. The intensity distribution of the low-frequency Os−N interval changes quite noticeably across the entire luminescence band. However, the simple harmonic three-mode model is able to reproduce the band shape very well, which is highlighted by the sloping lines on the first and fourth clusters. Because there was no apparent evidence for multiple transitions from different origins, a single-origin model was used to calculate the total spectrum. Figure 7b shows the experimental 6 K luminescence spectrum (top trace) and the best-fit calculated spectrum (bottom trace) of the **PPN** compound. This spectrum was calculated using the same a_{1g} vibrational modes as before and three origins based on the first peak of the main spectrum (12975 cm^{-1}) and at 12540 and 11980 cm^{-1}, which correspond to the 435 and 1000 cm^{-1} intervals discussed earlier. The total spectrum was obtained in a similar manner as for **TBA**, where the relative intensity of the first peak in each spectrum was adjusted by multiplying the spectrum by an appropriate factor to reproduce the overall spectral band envelope, which qualitatively accounts for the intensities of each transition. The individual spectra are added to give the total calculated spectrum with the proper intensity ratios for each of the constituent spectra. Agreement between the experimental and calculated spectra is very good; however, all of the fine resolved features, such as lattice modes, cannot be reproduced entirely.

Emitting-State Displacements in the O═Os═O and CS High-Frequency Vibrational Modes. The normal-coordinate offsets used in the calculations are listed in Table 2 for each compound and are given in dimensionless units (Δ) and converted to Å (ΔQ). We compare the ΔQ values for the title compounds. The values for the emitting-state offset along the a_{1g} CS mode (ΔQ_{CS}) and the a_{1g} O═Os═O stretching mode ($\Delta Q_{O=Os=O}$) were 0.038 and 0.062 Å, respectively, for **TBA** and 0.060 and 0.065 Å, respectively, for **PPH**, demonstrating that the dominant displacement occurs along the CS mode. The larger offsets along the CS modes lead to a high-frequency interval closer to the CS frequency, which can be understood using an expression for predicting MIME frequencies (Supporting Information). Because the high-frequency interval in the **PPN** complex (880 cm^{-1}) was closer to the O═Os═O stretching frequency of 885 cm^{-1}, it is expected that $\Delta Q_{O=Os=O}$ (0.063 Å, I and II) should be larger than ΔQ_{CS} (0.061 Å). The value of $\Delta Q_{O=Os=O}$ for **TBA** was considerably smaller than those obtained from the other compounds. It is not apparent from the crystal structure of this compound if intermolecular packing forces impede motion along this coordinate, thus leading to smaller offsets.

Emitting-state normal-coordinate displacements along the low-frequency a_{1g} Os−N stretching mode were substantially larger than the offsets determined for the high-frequency modes in the **TBA** and **PPH** compounds with values of 0.078 and 0.089 Å, respectively, whereas the **PPN** compound shows a much smaller offset of 0.058 Å in this mode. This can be seen directly in the experimental spectra where the first quantum of the progression in this mode is the most intense followed by less intense transitions in higher quanta of this mode, indicating a smaller emitting-state displacement. It is also interesting to note that the largest displacement along Q_{Os-N} coincides with the largest value of ΔQ_{CS}, which leads to a high-frequency interval that more closely matches the frequency of the CS mode, such as in the **PPH** compound with a resolved high-frequency interval of 855 cm^{-1}. The **PPN** compound is at the other limit where smaller values of ΔQ_{Os-N} and smaller ΔQ_{CS} are obtained and a high-frequency interval (880 cm^{-1}) that is closer to the frequency of the O═Os═O mode of 885 cm^{-1}. This apparent correlation between the CS and Os−N stretching coordinates could arise from varying changes in the distribution of electron density across the Os−NCS fragment for each compound. This effect can be qualitatively understood from the molecular orbital surfaces presented in Figure 5, whereby a large change in electron density in the *xy* plane leads to larger values of both ΔQ_{Os-N} and ΔQ_{CS}. Comparisons of calculated ΔQ values with other *trans*-dioxo complexes are presented in the Supporting Information.

The detailed analysis of vibronic structure and extraction of emitting-state offsets for each displaced normal coordinate provides a valuable insight into the excited-state geometries of the title complexes and related *trans*-dioxo complexes. However, there is no conclusive evidence from these calculations for why the luminescence band shapes change so much between the compounds. Judging from the invariance of Raman frequencies for the O═Os═O, CS, and Os−N modes in the three compounds, the ligand spheres around the metal center are practically identical. The effect of the environment on the emitting-state properties of these compounds appears to have a significant influence on what is formally a metal-centered electronic transition. This interaction between intra- and intermolecular properties has also been observed in different salts of the *trans*-$[ReO_2(pyridine)_4]^+$ complex, for which luminescence band shapes and energies change somewhat as a function of counterion.[20,21]

Conclusions

The nonzero offsets of the emitting-state potential energy minima along a ligand-centered vibrational mode are illustrated in the *trans*-dioxo class of complexes for the first time. Judging from the values of normal-coordinate offsets extracted from the calculated luminescence spectra, it appears that the magnitude of the low-frequency (Os−N) normal-coordinate offset is related to that of the high-frequency CS mode. This interdependence of the metal−ligand and ligand-centered stretching motions is also supported by theoretical calculations, where calculated O═Os═O, CS, and Os−N symmetric stretching frequencies closely matched those observed in experimental vibrational spectra and all contained varying contributions from the Os═O, CS, and Os−N coordinates. The intramolecular luminescence transition also

(20) Newsham, M. D.; Giannelis, E. P.; Pinnavaia, T. J.; Nocera, D. G. *J. Am. Chem. Soc.* **1988**, *110*, 3885.
(21) Grey, J. K.; Butler, I. S.; Reber, C. *Can. J. Chem.*, in press, 2004.

appears to be influenced by the environment of the *trans*-$[OsO_2(NCS)_4]^{2-}$ luminophore, where the magnitudes of normal-coordinate offsets and luminescence energies change noticeably between compounds.

Acknowledgment. Funding for this work was provided from the Natural Sciences and Engineering Council (Canada) in the form of research grants and a postgraduate scholarship (J.K.G.).

Supporting Information Available: Electronic structures of *trans*-dioxo complexes. Wavelength-dependent luminescence spectra of **TBA**, vibronic analysis of low-temperature absorption spectra, resonance Raman excitation profiles, discussion of the MIME, comparison of normal-coordinate offsets with other *trans*-dioxo systems. This material is available free of charge via the Internet at http://pubs.acs.org.

IC049840V